Record Charge Carrier Diffusion Length in Colloidal Quantum Dot Solids via Mutual Dot-To-Dot Surface Passivation

Graham H. Carey, Larissa Levina, Riccardo Comin, Oleksandr Voznyy, and Edward H. Sargent*

Colloidal quantum dots (CQDs) offer a powerful platform for the fabrication of optoelectronic devices, including photodetectors,[1] photovoltaics,[2–4] and light-emitting diodes.[5,6] A key advantage of CQDs resides in the quantum confinement effect wherein the bandgap and optoelectronic properties can be tailored simply by adjusting the size of nanoparticle used.[7–9]

This flexibility brings with it a challenge compared with the case of typical bulk polycrystalline semiconductors. The CQD diameter (in, for example, PbS and PbSe) to achieve a ≈1.0–1.3 eV bandgap is in the range of 3–4 nm.[10,11] As a result, a large proportion of atoms making up the quantum dot are surface atoms that require careful termination in light of the crucial influence of nanocrystal surfaces on passivation and confinement.[12,13] Much of the work in this field has focused on passivating maximally these surface sites using ligands. Indeed, innovative strategies, including both molecular[3,14–17] and atomic[4,18,19] ligands, have recently led to considerable advances in in-gap trap state density and consequently solar cell performance. While considerable progress has been made, quantum dot surface passivation remains a significant limiter of film optoelectronic properties and device performance.[20]

Recent reports of partially fused quantum dot systems[21,22] hint at a possible new passivation strategy. Rather than passivate every surface site using extraneous chemical additives, we would seek to combine chemical passivation with partial fusing of certain surfaces presented by adjacent quantum dots. Our strategy (depicted in **Figure 1**a) would unite dot-to-dot surface-coupled self-passivation (to reduce the overall surface-to-volume ratio within the quantum dot solid) with strong chemical passivation of the remaining surface sites. We show herein that reducing the available surface area while strongly passivating remaining sites led to a very low density of electronic traps. We further show that, at the same time as excellent electronic transport was achieved, impressively long-lived excited-state lifetimes were simultaneously observed. The combination of excellent transport and reduced trapping led to the longest reported diffusion lengths observed in a colloidal quantum dot solid.

The aforementioned recent reports, in which quantum dots were partially connected, did not incorporate the most effective passivation strategies. Indeed, this was not an option, for the surface fusing was based on harsh processing conditions that stripped off all passivating ligands.

We, therefore, devised a new process that could allow partial facet fusing to be combined with excellent chemical surface passivation. It is based on a combination of a strongly bound atomic ligand, which serves to provide efficient passivation, and a more labile organic ligand, used only to ensure steric colloidal stabilization. Amine treatments have recently been deployed to create well-packed, connected, and highly conductive arrays of quantum dots.[22] We, therefore, developed a synthesis method designed to produce PbS quantum dots capped with amine ligands instead of oleic acid. The synthesis design was informed by recent reports of highly passivated, amine-stabilized CdSe quantum dots.[23–25] The synthesis is described in full in the Experimental Section; as shown in **Scheme 1**, CQDs are initially synthesized with oleic acid capping ligands, which are immediately replaced with chloride atomic ligands and tributylphosphine (PBu$_3$). A mixture of *n*-hexylamine and *n*-octylamine is then used to replace the PBu$_3$, balancing the need for ligands long enough to stabilize the nanocrystals in a standard organic solution, yet short enough to enable partial fusing during film formation. The ligand exchange was tracked via Fourier transform infrared (FTIR) spectroscopy; Figure S1 (Supporting Information) characterizes one representative dot batch at each stage of the exchange. In contrast with the previously reported exchange using CdSe CQDs, oleate is evident at all stages of the PbS CQD exchange until the final amine replacement step. X-ray photoelectron spectroscopy (XPS) measurements were performed on pristine, drop-cast films of the amine-exchanged PbS CQDs (Figure S2, Supporting Information), showing the presence of chloride ligands (Figure S2a, Supporting Information), and the full elimination of PBu$_3$ and oleate (Figure S2b,c, Supporting Information). We hypothesize that the PBu$_3$ and Me$_3$Si-Cl exchange steps partially replace oleic acid on the surface, providing initial surface chloride ligands and facilitating the final, full amine exchange required for subsequent facet fusing.

Using HRTEM, we investigated whether any quantum dot fusing occurred in the resultant films following film deposition and ligand exchange using 3-mercaptopropionic acid (MPA). Figure 1b shows the HRTEM images that, even at the very low concentrations required to generate a sub-monolayer of quantum dots, evidence partially fused dot clusters. The insets in Figure 1b show specific instances of two or more dots that have fused, and alignment in diffraction fringes is evident among multiple adjacent quantum dots. Such alignment

G. H. Carey, Dr. L. Levina, Dr. R. Comin, Dr. O. Voznyy, Prof. E. H. Sargent
Department of Electrical and Computer Engineering
University of Toronto, 10 King's College Road
Toronto, Ontario M5S 3G4, Canada
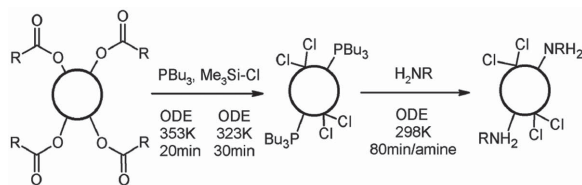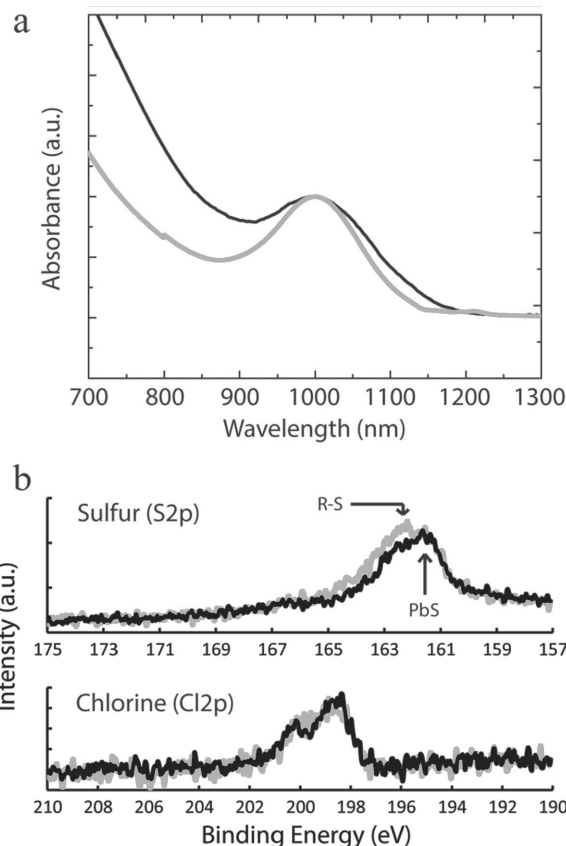E-mail: ted.sargent@utoronto.ca
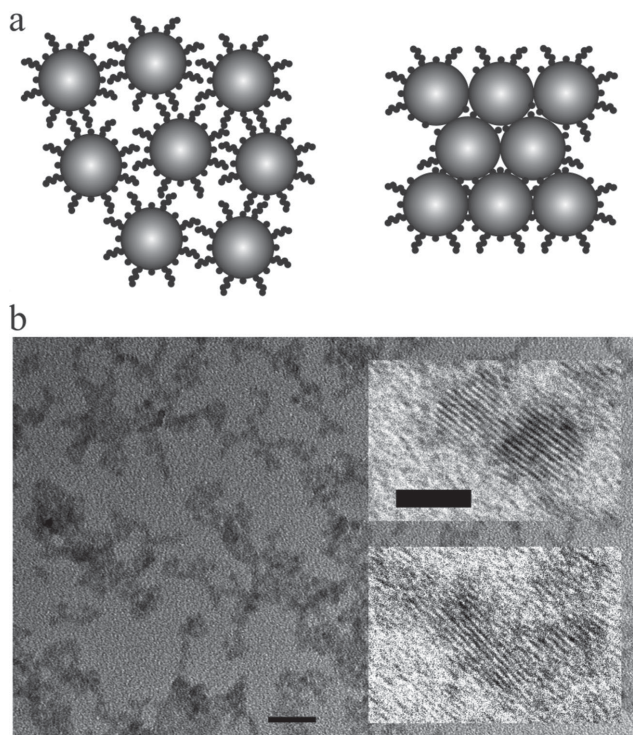
Figure 1. a) Schematic of a typical collection of colloidal quantum dots after ligand exchange when initially capped with oleic acid and chloride (left) or a short primary amine and chloride (right). Amine-capped dots allow partial fusing, reducing total available surface sites in a film. b) Transmission electron microscope image showing partial quantum dot fusing occurring—the insets show prominent instances of two or more dots fusing. Scale bars indicate 20 nm in the overview and 5 nm in the two inset images.

Figure 2. a) Absorbance (normalized to exciton peak) of amine-capped PbS quantum dots in solution (gray) and in film after ligand exchange with 3-mercaptopropionic acid and $CdCl_2$ (black). b) X-ray photoelectron spectra examining sulfur and chlorine characteristics in films of oleic acid (gray) or amine (black) capped quantum dots exchanged with 3-mercapto-propionic acid and $CdCl_2$. The arrows in the sulfur spectrum indicate the positions of lead-bound sulfur and ligand sulfur.

(oriented attachment) is a prerequisite for fusion to produce mutual passivation.

Further evidence of partial surface fusing was observed in full ligand-exchanged films. Films were fabricated using a layer-by-layer spin-coating approach; each layer of amine-capped PbS quantum dots was place-exchanged by treating with a solution of MPA mixed with a low concentration (0.2 mM) of $CdCl_2$. The goal of the inorganic metal halide salt was to retain and indeed improve halide passivation. Comparing absorption in solution to film absorption after ligand exchange (**Figure 2**a), we note two evident features. First, significant broadening has occurred, with a larger long-wavelength contribution after exchange, consistent with fusing within the film. Second, despite evidence of fusing, the excitonic feature is still relatively strong, indicating

that the exchange process has not eliminated the quantum confinement effect from the resulting film.

XPS measurements provide further support for fusing, as well as evidence of improved overall passivation. Control quantum dots (oleic acid/$CdCl_2$ passivated PbS) were compared with mutually passivated quantum dots (amine/chloride passivated PbS). Each film was treated with MPA and $CdCl_2$ as described above to maintain an equivalent number of chloride passivation steps; this is not expected to significantly impact the surface chemistry of control dots compared with a typical, MPA-only exchange. Figure S2d (Supporting Information) provides evidence from XPS measurements that the addition of $CdCl_2$ to the ligand exchange step does not affect the amount of chloride in a control dot film. Comparing mutually-passivated to control CQD films, it is observed that the thiol contribution to the sulfur 2p signal (left-hand contribution to sulfur signal in Figure 2b) is significantly reduced, consistent with reduced available surface area. By contrast, the chloride 2p signal is unchanged between the two treatment types, since atomic (chloride) ligands are less affected by the steric limitation of fused dot surfaces.

We interpret these stoichiometry data as promising with respect to the prospects for improved passivation. Fewer surface

Scheme 1. Synthesis of PbS-RNH_2-Cl colloidal quantum dots (mutually passivated PbS).

sites are available in the fused-surface case, since these surfaces are already occupied. Thus, having an equivalent density of chloride atoms in the film suggests a larger number of passivating halide anions per surface atom of the quantum dots, i.e., it points to the possibility of increased passivation density of the exposed facets.

We now turn to studies of minority carrier diffusion length (L_D), a key parameter most urgently in need of major progress in the field of CQD photovoltaics. We have shown recently that extending diffusion length will rely principally on reducing the density of deep electronic traps in CQD solids, while improving dot-to-dot transport will also offer advantages in the best present-day films.[20] We employed transient photoluminescence (PL) measurements to determine carrier diffusion lengths, for these methods have been extensively practiced in organic[26] and perovskite[27,28] semiconductors in very compelling recent reports. We would thereby directly compare control versus fused-and-passivated CQD films, and also benchmark our results to analogous reports in other materials systems.

The PL-based derivation of diffusion length relies on evaluating variation in the PL lifetime for pristine films (of known thickness) with and without a photoexcited-state-quenching interface. The dynamics and times scales of photogenerated carriers are subsequently interpreted within a 1D diffusion model in order to estimate the carrier lifetime and diffusion length.

CQD solids were formed via spin-coating on glass and were ligand-exchanged with MPA (control) or a mixture of MPA and $CdCl_2$ (mutually passivated), as described above. Unquenched films were prepared on bare glass, with film thicknesses of roughly 250 nm to ensure adequate PL signal and accurate carrier lifetime measurements. As shown in Figure S3 (Supporting Information), single-layer films exhibited an abnormally fast decay time, potentially attributable to cracks and voids, whereas thicker films exhibited minimal thickness dependence on decay time due to the infilling of cracks by subsequently deposited layers. Quenched films were prepared by spin-coating an electron-accepting layer of phenyl-C_{61}-butyric acid methyl ester (PCBM) on titanium dioxide, and then depositing a two-quantum dot layers (50 ± 5 nm and 75 ± 5 nm for the control and mutually-passivated films, respectively). The thickness was chosen to fall below expected diffusion length in each case in order to ensure a sizable quenching effect. In all cases, the pulsed excitation source (633 nm) was incident on the CQD film side. Steady-state photoluminescence measurements (Figure S4, Supporting Information) were used to determine the emission wavelength of interest for subsequent decay measurements (1110 nm for control dots, 1225 nm for mutually-passivated dots).

Time-resolved PL decay measurements are shown in **Figure 3**, along with two-component exponential fits to each data set, representing a fast exciton dissociation time constant and a slower transport-assisted recombination lifetime. The fast, but not resolution-limited, exponential component was accurately determined by fitting data measured on a smaller time window (Figure S5, Supporting Information). The carrier lifetimes for each case are reported and compared in **Table 1**; even before evaluating the results within the framework of the diffusion model, one readily observes that the mutual-passivation method leads to a doubling of carrier lifetime compared with
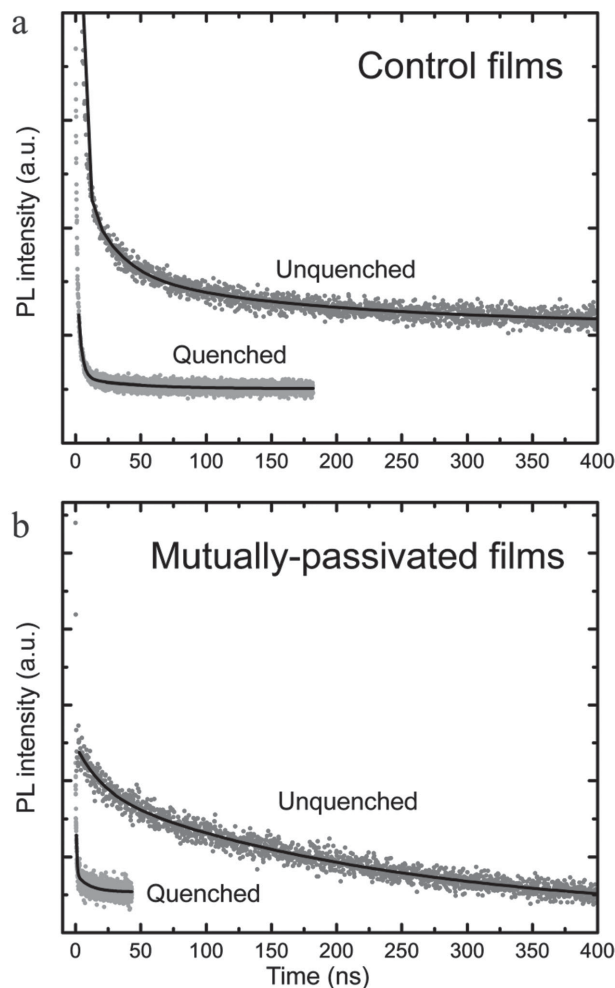
Figure 3. Photoluminescence lifetime measurements of MPA-exchanged films of a) control PbS quantum dots and b) mutually passivated PbS quantum dots. The dark gray points represent data for thick (>200 nm) films on glass, while the light gray points represent thin films (50 and 75 nm, respectively) on a quenching layer of PCBM/titanium dioxide.

the control. At the same time, it produces a significantly shorter quenching lifetime, suggesting the sought-after improved transport.

Full details on the diffusion model applied to the PL decay results can be found in previous reports;[28] in brief, the dynamics are modeled using a 1D diffusion equation (Equation 1)

$$\frac{\partial n(x,t)}{\partial t} = D\frac{\partial^2 n(x,t)}{\partial x^2} - k(t)n(x,t) \qquad (1)$$

Table 1. Electrical carrier transport figures of merit.

	Unquenched lifetime [ns]	Quenched lifetime [ns]	Diffusion length [nm]	Mobility [$cm^2\ V^{-1}\ s^{-1}$]	Exciton dissociation rate [ns^{-1}]
Control	148 ± 4	24 ± 3	70 ± 10	1×10^{-2}	2.0 ± 0.1
Mutually passivated	268 ± 5	11 ± 1	230 ± 20	8×10^{-2}	3.7 ± 0.1

COMMUNICATION

where D is the diffusion coefficient and k represents the unquenched PL decay rate. Equation 1 is solved for the time- and depth-dependent carrier concentration by assuming appropriate boundary conditions, i.e., that all carriers at the quantum dot/PCBM interface are quenched, leading to the condition $n(L, t) = 0$, where L is the film thickness, and that the carrier population outside the film is zero, i.e., $n(x, t) = 0$, for $x < 0$. Additionally, the initial excitation distribution can be written as $n(x, 0) = n_0 \exp(-\alpha x)$, where α is the absorption coefficient at the excitation wavelength. Absorption coefficients for each film were extracted from Figure S6 (Supporting Information).

As previously reported, this model can be simplified to a plot of diffusion length in units of film thickness against the ratio between quenched and unquenched PL lifetimes (Figure S7, Supporting Information). Plotting the two observed lifetime ratios on this curve leads to an estimated diffusion length of 70 ± 10 nm for the control, and of 230 ± 20 nm for the mutually-passivated films. From the relation $L_D = \sqrt{D\tau}$ as well as Einstein's relation (Equation 2), the effective electron mobility can also be estimated for each film. Diffusion length and mobility are reported together with carrier lifetime measurements and estimated exciton dissociation rates in Table 1

$$D = \frac{\mu k_B T}{q} \tag{2}$$

The threefold improvement in diffusion length compared with control films represents the highest reported diffusion length to date in colloidal quantum dot solids. This measured value is comparable to diffusion lengths in those perovskite films typically utilized in mesoporous electrodes, although shorter than the longest L_D values reported and employed in planar perovskite architectures.

A compelling example application of a significantly longer diffusion length is the realization of a photovoltaic device that can exploit a notably thicker light-absorbing layer, enabling a higher current density and maintaining fill factor. For control films, it has been previously reported that the optimal film thickness is typically in the range of 300 nm, beyond which any minimal gains in current density are more than offset by a loss in fill factor. By contrast, devices prepared using the mutual-passivation method were found to have an optimal thickness of 600 nm. Electrical characterization of a hero device is shown in **Figure 4**a; fill factor for the thick device is comparable to that of standard-thickness control devices (58% fill factor), while the additional 300 nm of absorptive material allows the generation of just below 30 mA cm^{-2} in current density (confirmed by external quantum efficiency measurements, Figure 4b). While open-circuit voltage is somewhat lower than control devices (likely explained by the red-shift due to fusing observed in Figure 4b), the power conversion efficiency is 9.2%.

The dot-to-dot mutual surface passivation approach, when combined with the best available methods in quantum dot chemical passivation, leads to the formation of films with diffusion lengths fully three times longer than previously reported quantum dot solids. Applying this materials processing approach to photovoltaic devices allows for thicker optimized films, with significant increases in photocurrent and negligible fill factor loss. Additionally, the approach
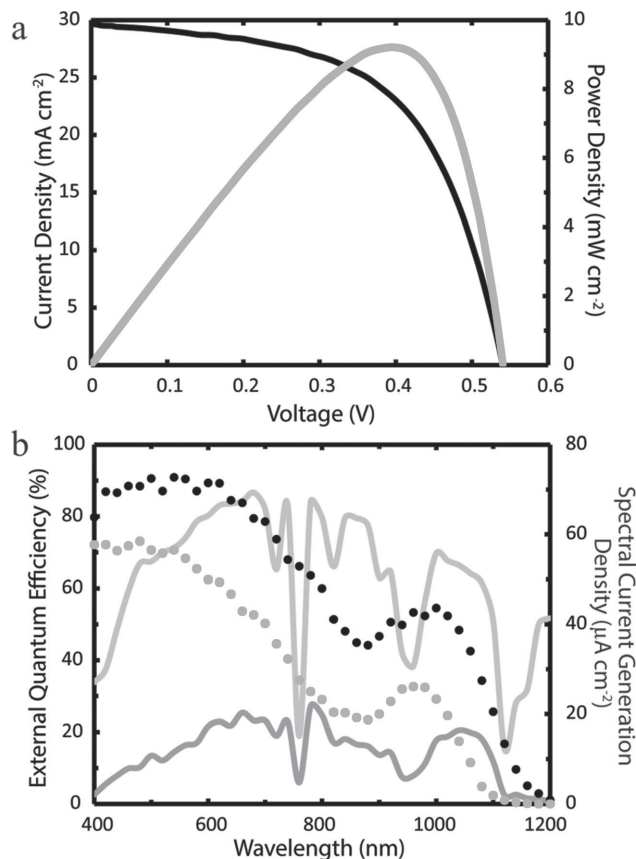
Figure 4. a) Current (black) and power (gray) density versus applied bias measurements for a high diffusion length film (thickness 600 nm), with maximum power point power conversion efficiency of 9.2%. b) External quantum efficiency measurements for thickness-optimized control films (gray circles, calculated current 21.6 mA cm^{-2}) and mutually passivated films (black circles, calculated current 29.5 mA cm^{-2}). Total spectral current generation density for a hypothetical 100% EQE device is shown (upper solid curve); additional spectral current density gained by the mutually passivated devices compared with control is shown by the lower solid curve.

offers a robust platform for interesting future applications; low trap density and long diffusion length are desirable qualities when constructing high-performance current-matched tandem photovoltaic devices, either fully CQD-based or as efficient IR conversion in conjunction with crystalline semiconductor cells.

Experimental Section

Colloidal Quantum Dot (CQD) Synthesis: Control PbS quantum dots were synthesized according to a previously published method,[29] using a previously reported in-synthesis halide treatment.[3] PbS CQD for mutual passivation studies were synthesized using a slight variant of the aforementioned method: after the growth of oleic acid-capped CQD of desired size (omitting the in-synthesis CdCl$_2$ treatment), tributylphosphine was injected during the reaction cooling process, with injection at 80 °C and 20 min reaction time. Trimethylchlorosilane was injected at 50 °C, with a 30 min reaction time. After the reaction vessel cooled to 30 °C, the quantum dot solution aggregated; the supernatant was removed and the reaction vessel was refluxed with argon. Subsequently, *n*-hexylamine was injected (stirring 80 min) followed by

n-octylamine for an additional 80 min stirring. Following full reaction, the CQD solution was precipitated with methyl acetate, dried for 16 h under mild vacuum, and redispersed at roughly 100 mg mL^{-1} in octane. All reagents were purchased from Sigma Aldrich.

CQD Film Fabrication and Ligand Exchange: CQD films were prepared on glass (for spectroscopy and PL studies) or TiO$_2$ electrodes (for photovoltaic devices; 50 nm of TiO$_2$ sputtered on fluorine-doped tin oxide (FTO)-coated glass) using layer-by-layer spin-coating deposition under ambient conditions. Control films were deposited from a 50 mg mL^{-1} solution of quantum dots in octane at 2500 rpm to obtain layers of roughly 25 nm thickness, while amine-capped CQD were deposited from a 100 mg mL^{-1} solution in octane, spun at 2500 rpm to generate roughly 35 nm thick layers. Each layer was treated with 1% 3-mercaptopropionic acid (MPA) in methanol (v/v); for mutually-passivated films, the MPA solution included 0.2 mM CdCl$_2$. All films prepared for XPS measurements (control and mutually-passivated) were exchanged with an MPA/CdCl$_2$ solution to maintain a consistent number of Cl-passivation steps. All films were rinsed with pure methanol after ligand exchange, spinning at 2500 rpm after each rinse. For photovoltaic devices, top electrodes were deposited by thermal and electron beam evaporation, and consisted of 40 nm of MoO$_3$, 50 nm of gold, and 150 nm of silver, deposited at a rate of 0.2 (thermal MoO$_3$), 0.4 (electron beam Au), and 1 (thermal Ag) Å s^{-1}, at a pressure of <1 × 10^{-6} mbar.

Materials Characterization: The surface elements and chemical states of the PbS CQD films were analyzed using X-ray photoelectron spectroscopy (XPS) (PHI-5500). A monochromated Al K radiation source (1486.7 eV) was used to excite photoelectrons in an ultrahigh vacuum atmosphere at ≈10^{-9} Torr. The binding energy scale was calibrated using the Au 4f 7/2 peak at 83.98 eV and the Cu 2p 3/2 peak of sputter-cleaned Cu at 932.67 eV.

Transient Photoluminescence: Transient PL measurements were performed in reflection geometry (at an incidence angle of 30° from the sample surface to avoid spurious reflections of the incident light) using a 633 nm laser diode as a pulsed excitation source (with a temporal profile of ≈0.13 ns), in combination with a double-grating spectrometer. The time traces were acquired using a time-correlated single-photon-counting (TCSPC) near-infrared detector (air-cooled photomultiplier tube). The time window was set according to the measured timescale in order to ensure a complete decay of the photogenerated carriers between consecutive excitation pulses.

Photovoltaic Performance Characterization: Current–voltage data were measured with the device at ambient temperature in a constantly purged nitrogen environment, using a Keithley 2400 source meter. The solar spectrum at AM1.5 was simulated to within class A specifications (less than 25% spectral mismatch) with a xenon lamp and filters (ScienceTech; measured intensity of 100 mW cm^{-2}). The source intensity was measured with a Melles–Griot broadband power meter through a circular 0.049 cm^2 aperture. The same aperture was used in device measurements; the aperture is slightly smaller than the top device electrode to avoid overestimating photocurrent. The entire photon fluence passing through the aperture was counted as incident on the device for all current analyses. The spectral mismatch of the system was characterized using a calibrated reference solar cell (Newport). The total AM 1.5 spectral mismatch—taking into account the simulator spectrum and the spectral responsivities of the test cell, reference cell, and broadband power meter—was remeasured periodically and found to be ≈9.4%. This multiplicative factor, $M = 0.906$, was applied to the current density values of the J–V curve to most closely resemble true AM 1.5 performance.[30] External quantum efficiency measurements were obtained by applying chopped (220 Hz) monochromatic illumination (450 W xenon lamp through a monochromator with order-sorting filters) collimated and cofocused with a 0.7 sun intensity white light source on the device of interest. The power was measured with calibrated Newport 818-UV and Newport 818-IR power meters. The response from the chopped signal was measured using a Stanford Research system current preamplifier feeding into a Stanford Research system lock-in amplifier set to voltage mode.

Supporting Information

Supporting Information is available from the Wiley Online Library or from the author.

Acknowledgements

[1] G. Konstantatos, I. Howard, A. Fischer, S. Hoogland, J. Clifford, E. Klem, L. Levina, E. H. Sargent, *Nature* **2006**, *442*, 180.

[2] S. A. McDonald, G. Konstantatos, S. Zhang, P. W. Cyr, E. J. D. Klem, L. Levina, E. H. Sargent, *Nat. Mater.* **2005**, *4*, 138.

[3] A. H. Ip, S. M. Thon, S. Hoogland, O. Voznyy, D. Zhitomirsky, R. Debnath, L. Levina, L. R. Rollny, G. H. Carey, A. Fischer, K. W. Kemp, I. J. Kramer, Z. Ning, A. J. Labelle, K. W. Chou, A. Amassian, E. H. Sargent, *Nat. Nanotechnol.* **2012**, *7*, 577.

[4] C.-H. M. Chuang, P. R. Brown, V. Bulović, M. G. Bawendi, *Nat. Mater.* **2014**, *13*, 796.

[5] J. S. Steckel, S. Coe-Sullivan, V. Bulović, M. G. Bawendi, *Adv. Mater.* **2003**, *15*, 1862.

[6] L. Qian, Y. Zheng, J. Xue, P. H. Holloway, *Nat. Photonics* **2011**, *5*, 543.

[7] C. B. Murray, D. J. Norris, M. G. Bawendi, *J. Am. Chem. Soc.* **1993**, *115*, 8706.

[8] X. Wang, G. I. Koleilat, J. Tang, H. Liu, I. J. Kramer, R. Debnath, L. Brzozowski, D. A. R. Barkhouse, L. Levina, S. Hoogland, E. H. Sargent, *Nat. Photonics* **2011**, *5*, 480.

[9] O. E. Semonin, J. M. Luther, S. Choi, H.-Y. Chen, J. Gao, A. J. Nozik, M. C. Beard, *Science* **2011**, *334*, 1530.

[10] L. Cademartiri, E. Montanari, G. Calestani, A. Migliori, A. Guagliardi, G. A. Ozin, *J. Am. Chem. Soc.* **2006**, *128*, 10337.

[11] I. Moreels, K. Lambert, D. Smeets, D. De Muynck, T. Nollet, J. C. Martins, F. Vanhaecke, A. Vantomme, C. Delerue, G. Allan, Z. Hens, *ACS Nano* **2009**, *3*, 3023.

[12] J. Mooney, M. M. Krause, J. I. Saari, P. Kambhampati, *Phys. Rev. B: Condens. Matter Mater. Phys.* **2013**, *87*, 081201.

[13] P. Kambhampati, *Chem. Phys.* **2015**, *446*, 92.

[14] C. Giansante, L. Carbone, C. Giannini, D. Altamura, Z. Ameer, G. Maruccio, A. Loiudice, M. R. Belviso, P. D. Cozzoli, A. Rizzo, G. Gigli, *J. Phys. Chem. C* **2013**, *117*, 13305.

[15] D. Kim, D.-H. Kim, J.-H. Lee, J. Grossman, *Phys. Rev. Lett.* **2013**, *110*, 196802.

[16] J. M. Luther, M. Law, Q. Song, C. L. Perkins, M. C. Beard, A. J. Nozik, *ACS Nano* **2008**, *2*, 271.

[17] A. Fischer, L. Rollny, J. Pan, G. H. Carey, S. M. Thon, S. Hoogland, O. Voznyy, D. Zhitomirsky, J. Y. Kim, O. M. Bakr, E. H. Sargent, *Adv. Mater.* **2013**, *25*, 5742.

[18] Z. Ning, O. Voznyy, J. Pan, S. Hoogland, V. Adinolfi, J. Xu, M. Li, A. R. Kirmani, J.-P. Sun, J. Minor, K. W. Kemp, H. Dong, L. Rollny,

A. Labelle, G. Carey, B. Sutherland, I. Hill, A. Amassian, H. Liu, J. Tang, O. M. Bakr, E. H. Sargent, *Nat. Mater.* **2014**, *13*, 822.

[19] J. Tang, K. W. Kemp, S. Hoogland, K. S. Jeong, H. Liu, L. Levina, M. Furukawa, X. Wang, R. Debnath, D. Cha, K. W. Chou, A. Fischer, A. Amassian, J. B. Asbury, E. H. Sargent, *Nat. Mater.* **2011**, *10*, 765.

[20] D. Zhitomirsky, O. Voznyy, L. Levina, S. Hoogland, K. W. Kemp, A. H. Ip, S. M. Thon, E. H. Sargent, *Nat. Commun.* **2014**, *5*.

[21] W. J. Baumgardner, K. Whitham, T. Hanrath, *Nano Lett.* **2013**, *13*, 3225.

[22] C. S. S. Sandeep, J. M. Azpiroz, W. H. Evers, S. C. Boehme, I. Moreels, S. Kinge, L. D. A. Siebbeles, I. Infante, A. J. Houtepen, *ACS Nano* **2014**, *8*, 11499.

[23] N. C. Anderson, J. S. Owen, *Chem. Mater.* **2012**, *25*, 69.

[24] N. C. Anderson, M. P. Hendricks, J. J. Choi, J. S. Owen, *J. Am. Chem. Soc.* **2013**, *135*, 18536.

[25] Z. M. Norman, N. C. Anderson, J. S. Owen, *ACS Nano* **2014**, *8*, 7513.

[26] P. E. Shaw, A. Ruseckas, I. D. W. Samuel, *Adv. Mater.* **2008**, *20*, 3516.

[27] S. D. Stranks, G. E. Eperon, G. Grancini, C. Menelaou, M. J. P. Alcocer, T. Leijtens, L. M. Herz, A. Petrozza, H. J. Snaith, *Science* **2013**, *342*, 341.

[28] G. Xing, N. Mathews, S. Sun, S. S. Lim, Y. M. Lam, M. Grätzel, S. Mhaisalkar, T. C. Sum, *Science* **2013**, *342*, 344.

[29] M. A. Hines, G. D. Scholes, *Adv. Mater.* **2003**, *15*, 1844.

[30] H. J. Snaith, *Nat. Photonics* **2012**, *6*, 337.